Evaluation of the Factors Determining HBT High-Frequency Performance by Direct Analysis of *S*-Parameter Data

David R. Pehlke and Dimitris Pavlidis, *Senior Member, IEEE*

***Abstract*—A novel parameter extraction formalism for the evaluation of Heterojunction Bipolar Transistor (HBT) device physics is presented. The technique employs analytically derived expressions for direct calculation of the HBT T-Model equivalent circuit element values in terms of the measured *S*-parameters. All elements are directly calculated with the exception of the emitter leg of the T-model. This approach avoids errors due to uncertainty in fitting to large, overdetermined equivalent circuits and does not require the use of test structures and extra measurement steps to evaluate parasitics. Detailed bias dependent results for the directly calculated circuit elements are presented. An analysis is also reported of the short circuit current gain that separates the transit times and RC products and allows evaluation of their individual contribution to the measured f_T and significance in limiting the HBTs high frequency performance.**

I. Introduction

HBTs have recently demonstrated significantly improved RF performance into the mm-wave frequencies with the advent of self-aligned technologies, innovative isolation approaches to reduce parasitic effects, and exploitation of ballistic transport in the base-collector depletion region. As these technologies mature and parasitic resistances and capacitances are minimized, it becomes increasingly important to analyze the exact causes of device limitations in terms of the HBT device physics and equivalent circuit representation. By studying the impact of particular transit times, resistances and capacitances on the device performance, we may then apply technologies to best optimize those aspects that limit the device performance. Fitting routines to numerically optimize relatively large equivalent circuits to match measured data may result in non-unique solutions for element values that depend on starting conditions [1]. Many laboratories have developed parameter extraction techniques for high-frequency devices [2], [3]. However, even the best of those approaches require some separate measurement of test structures to characterize parasitics, whose effect is then mathematically subtracted out before calculating the intrinsic circuit, whereas the approach developed by the authors [4] does not require this.

This paper presents further details of the direct calculation of the HBT equivalent circuit from *S*-parameter measurements and an insight into the factors determining the f_T characteristics of the HBT. The formalism of direct calculation of the HBT equivalent circuit from *S*-parameter measurements is presented in Section II. Detailed bias-dependent results of base resistance, collector resistance, base-collector capacitance, frequency dependence of $\alpha(\omega)$, and exact values of base and collector transit times are discussed in Section III using the proposed new technique. The expression for H_{21} in terms of the equivalent circuit element values is evaluated in Section IV to determine the components most responsible for its roll-off to the f_T intercept at $|H_{21}| = 1$. The technique allows separation of transit time and RC factors so that individual contributions may be isolated and evaluated. This allows insight into exactly which elements are most important to target in technological optimization for high speed performance.

II. Formalism for Direct Extraction of HBT Equivalent Circuit Parameters

The GaAs/AlGaAs HBTs characterized in this work were fabricated at the University of Michigan using a self-aligned technology allowing 0.1 μm separation between base ohmic metal and active emitter [5]. The MOCVD-grown device layer structure consists of a 1500 Å GaAs emitter cap doped n^+ ($2 \cdot 10^{18}/\text{cm}^3$), 1000 Å $Al_{0.3}Ga_{0.7}As$ emitter layer doped n ($2 \cdot 10^{17}/\text{cm}^3$), 1000 Å GaAs base layer doped p^+ ($1 \cdot 10^{19}/\text{cm}^3$), 1.5 μm GaAs pre-collector layer doped n^- ($1 \cdot 10^{16}/\text{cm}^3$), and 1.0 μm GaAs collector doped n^+ ($2 \cdot 10^{18}/\text{cm}^3$) all grown on semi-insulating substrate. The base-emitter and base-collector active areas were 415 μm^2 and 1335 μm^2 respectively.

The HBT equivalent circuit used for this work is the conventionally accepted T-model shown in Fig. 1 along with a table of calculated element values using our method. The approach presented in this paper allows the evaluation of the impedances corresponding to the outlined circuit blocks in Fig. 1. No pad parasitic capacitances on the input or output ports were included in the

Manuscript received March 31, 1992; revised July 28, 1992. This work was supported by the Army Research Office (Contract No. DAAL03-92-G-0109).

The authors are with Solid-State Electronics Laboratory, Department of Electrical Engineering and Computer Science, University of Michigan, 1301 Beal Avenue, Ann Arbor, Michigan 48109-2122.

IEEE Log Number 9203694.

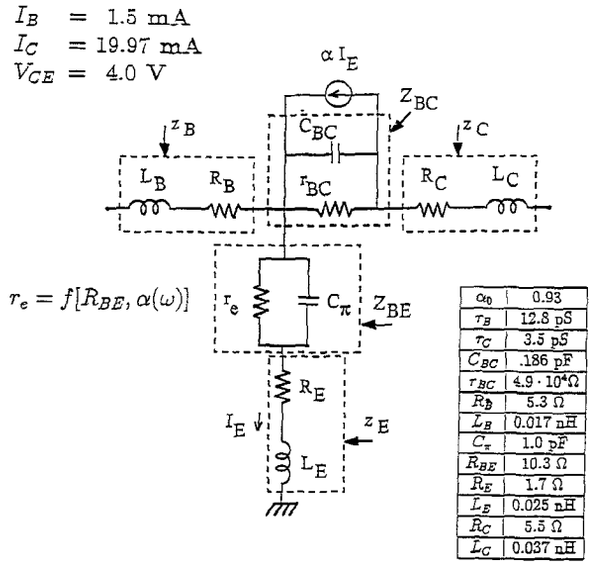

α_0	0.93
τ_B	12.8 pS
τ_C	3.5 pS
C_{BC}	.186 pF
r_{BC}	$4.9 \cdot 10^4\Omega$
R_B	5.3 Ω
L_B	0.017 nH
C_π	1.0 pF
R_{BE}	10.3 Ω
R_E	1.7 Ω
L_E	0.025 nH
R_C	5.5 Ω
L_C	0.037 nH

Fig. 1. HBT T-model equivalent circuit and parameters extracted using the proposed technique.

equivalent circuit model for this work. The extrinsic capacitances to ground are small for the devices tested which were laid out for on-wafer probing. Furthermore, they are not suspected to significantly influence the results presented here based on the analysis presented, the excellent correspondence of this model with the measured *S*-parameter data, and the relatively low frequency range of operation for this device. Information on the individual elements contained in these blocks can be obtained by examining the frequency dependences of the block impedance. The HBT extrinsic *H*-parameter formulation for the equivalent circuit of Fig. 1 is

$$H_{11} = z_B + \frac{(Z_{BE} + z_E)(Z_{BC} + z_C)}{(Z_{BE} + z_E + z_C) + Z_{BC}(1 - \alpha)} \quad (1)$$

$$H_{21} = \frac{\alpha Z_{BC} - (Z_{BE} + z_E)}{(Z_{BE} + z_E + z_C) + Z_{BC}(1 - \alpha)} \quad (2)$$

$$H_{12} = \frac{Z_{BE} + z_E}{(Z_{BE} + z_E + z_C) + Z_{BC}(1 - \alpha)} \quad (3)$$

$$H_{22} = \frac{1}{(Z_{BE} + z_E + z_C) + Z_{BC}(1 - \alpha)}. \quad (4)$$

And the solution of the impedance blocks of Fig. 1 may then be calculated in terms of the extrinsic common emitter *H*-parameters as

$$z_B = \frac{H_{11}H_{22} - H_{12}H_{21} - H_{12}}{H_{22}} \quad (5)$$

$$Z_{BC} + z_C = \frac{1 + H_{21}}{H_{22}} \quad (6)$$

$$Z_{BE} + z_E = \frac{H_{12}}{H_{22}} \quad (7)$$

$$\alpha Z_{BC} = \frac{H_{21} + H_{12}}{H_{22}}. \quad (8)$$

For the purpose of our calculations, the measured *S*-parameters are converted to *H*-parameters. The circuit elements contained in each of the above impedance blocks are then extracted by studying the frequency dependent characteristics of the particular block as explained below.

III. Application of the Technique to Direct Extraction of the HBT Equivalent Circuit Elements

The self-aligned GaAs/AlGaAs HBTs were measured from 0.5 GHz to 26 GHz using a Cascade Microtech on-wafer probe station and hp8510 Network Analyzer. Once the *S*-parameters are measured, the individual circuit element values are easily found by analyzing the above formulas. Examples of the parameters extracted in this way are discussed below.

A. Base Resistance (R_B) and Inductance (L_B)

From Fig. 1, we see that the form of z_B is that of a series R–L circuit which may be represented by

$$z_B = R_B + j\omega L_B. \quad (9)$$

By calculating z_B from equation (5) using the measured H_{ij} parameters, we pull out the base resistance, R_B, as its real part. Fig. 2 shows the values of base resistance calculated directly from these measurements have a slight bias dependence on injection level, and decrease slightly as the base current injection level is increased. These results provide good physical insight into the three components that make up the total R_B:

$$R_B = r_{B\Omega} + r_{BS} + r_B \quad (10)$$

where $r_{B\Omega}$ is the base ohmic metal contact resistance, r_{BS} is the series access component of the base resistance, and r_B is the active device spreading resistance. $r_{B\Omega}$ and r_{BS} are bias independent, while r_B should decrease as the collector current in the HBT is increased, resulting in the trend as seen in Fig. 2. The figure shows, however, that even when the device is heavily biased at $I_B = 2.5$ mA, the net decrease in R_B reflects the fact that most of the base resistance is made up of bias independent components. The series base inductance, L_B, is found in a similar way from the imaginary part of (5) and is shown in Fig. 3, as well as entered in the results of Fig. 1. The results of Fig. 3 for L_C will be discussed later in Section III-C.

B. Collector Resistance (R_C)

The parallel R–C circuit of Z_{BC} in series with the R–L circuit of z_C shown in Fig. 1 may be mathematically expressed as:

$$Z_{BC} + z_C = \left[R_C + \frac{r_{BC}}{1 + \omega^2 r_{BC}^2 C_{BC}^2}\right] + j\left[\omega L_C - \frac{\omega r_{BC}^2 C_{BC}}{1 + \omega^2 r_{BC}^2 C_{BC}^2}\right]. \quad (11)$$

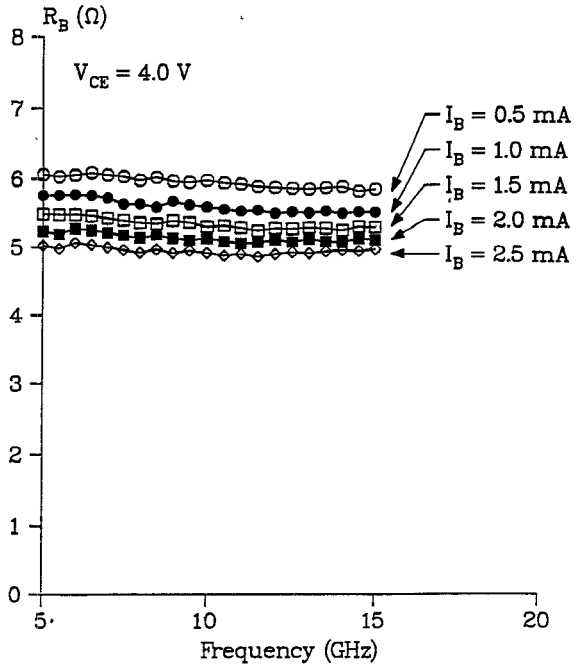

Fig. 2. Base resistance versus frequency showing the reduction of base resistance as the injection level is increased

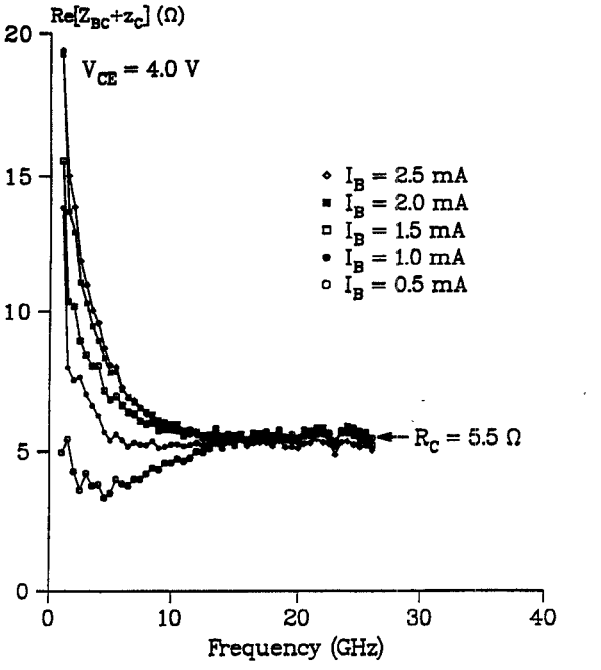

Fig. 4. Collector resistance versus frequency showing the bias independent behavior of the collector series access resistance.

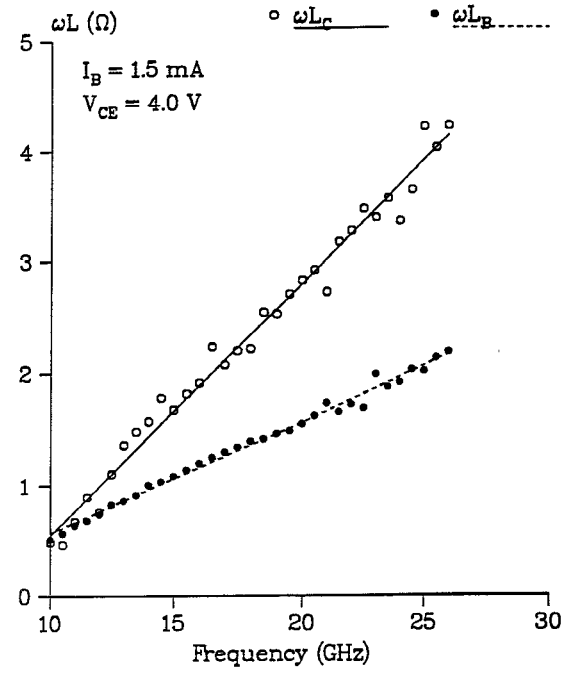

Fig. 3. ωL product versus frequency comparing the base and collector inductances.

At higher frequencies, where

$$\omega \gg \frac{1}{\sqrt{R_C r_{BC} C_{BC}^2}} \tag{12}$$

the real part of (11) decays to the value of the collector resistance, R_C, and the bias dependence of this is shown in Fig. 4. We see that the value of R_C arrived at is independent of injection levels as is expected for this series access resistance.

C. Base-Collector Capacitance (C_{BC}) and Collector Inductance (L_C)

The imaginary part of $Z_{BC} + z_C$ shown in (11) is dominated by C_{BC} at low frequencies. This is due to the large isolation resistance, r_{BC}, causing the imaginary part of $Z_{BC} + z_C$ to asymptotically approach $-1/\omega C_{BC}$ as the frequency becomes small, leaving us with a means for calculating C_{BC}:

$$C_{BC} = -\left(\omega \operatorname{Im}\left[\frac{1 + H_{21}}{H_{22}}\right]\right)^{-1} \tag{13}$$

$$\omega \ll \frac{1}{\sqrt{L_C C_{BC}}}. \tag{14}$$

In the case of devices tested here, this condition on the frequency applies below approximately 5 GHz and C_{BC} can be pulled out directly as seen in Fig. 5 as a function of V_{CE}. The C_{BC} value is found to drop in a square root dependence with applied reverse bias across the base-collector junction as is theoretically expected. The results vary less than 1% across this 1 GHz–5 GHz frequency band. These values directly calculated from S-parameters are compared in Table I with depletion approximation estimates based on the layer structure doping and base-collector active area. At higher frequencies, both C_{BC} and L_C contribute to the imaginary part of $Z_{BC} + z_C$, and once C_{BC} is determined, L_C can be found according to

$$L_C = \frac{1}{\omega} \operatorname{Im}\left[\frac{1 + H_{21}}{H_{22}}\right] + \frac{1}{\omega^2 C_{BC}} \tag{15}$$

and is compared with L_B in Fig. 3 (also see results of Fig. 1).

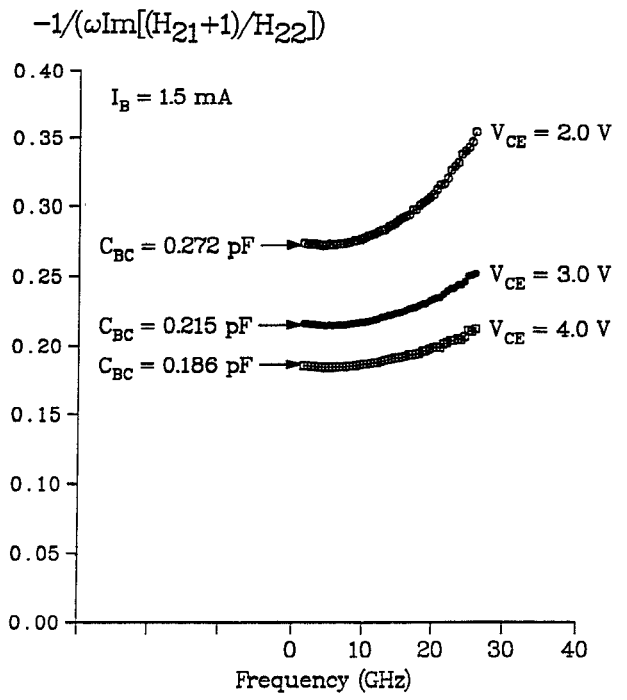

Fig. 5. Base-collector capacitance versus frequency at $I_B = 0.5$ mA showing the expected decrease in C_{BC} as V_{CE} is increased.

TABLE I
DIRECT EXTRACTION RESULTS FOR C_{BC} AND τ_C VERSUS DEPLETION APPROXIMATION ESTIMATES

V_{CE} (V)	S-Parameter Calculation C_{BC} (pF)	Depletion Approximation C_{BC} (pF)	S-Parameter Calculation τ_C (pS)	Depletion Approximation τ_C (pS)
2.0	.272	.271	1.8	2 8
3.0	.215	.225	3.0	3.4
4.0	.186	.197	4.0	3.9

D. Base-Collector Isolation Resistance (r_{BC})

The real part of $Z_{BC} + z_C$ as described in (11) becomes simplified at lower frequencies as the impedance of the base-collector capacitance C_{BC} starts to increase and it becomes a much less efficient feed-through element. We then start to see the effect of the large isolation resistance r_{BC} in parallel with it, and the real part of $Z_{BC} + z_C$ increases dramatically, with the real part of equation (11) becoming much larger than the collector series resistance R_C. This simplification of expression (11) occurs for frequencies below approximately 2–3 GHz in our devices, and the condition on ω may be described by

$$\omega \ll \frac{1}{\sqrt{R_C r_{BC} C_{BC}^2}}. \tag{16}$$

Under this low frequency condition, and by accounting for the fact that $r_{BC} >> R_C$, (11) can be reduced to a form that allows the calculation of r_{BC} as

$$r_{BC} = \left(\omega^2 C_{BC}^2 \operatorname{Re}\left[\frac{1 + H_{21}}{H_{22}}\right]\right)^{-1}. \tag{17}$$

In order to accurately extract r_{BC}, it is critical to measure device results at frequencies low enough to see the region where r_{BC} dominates this behavior (see results of Fig. 1 for the r_{BC} value of the tested device).

E. Base Transport Factor ($\alpha(\omega)$)

The base transport factor, $\alpha(\omega)$, can be calculated once C_{BC} is known by realizing that the latter dominates the imaginary part of Z_{BC} in (8). Because the isolation resistance, r_{BC}, is so large we can write

$$\omega C_{BC} >> \frac{1}{r_{BC}}. \tag{18}$$

Then by re-writing αZ_{BC} in terms of its circuit elements:

$$\alpha Z_{BC} = (\alpha_r + j\alpha_i)\left(\frac{1}{\frac{1}{r_{BC}} + j\omega C_{BC}}\right)$$

$$\approx (\alpha_r + j\alpha_i)\left(\frac{-j}{\omega C_{BC}}\right) \tag{19}$$

where α_r and α_i are the real and imaginary parts of the base transport factor, respectively. From (8) and (19) one can calculate $\alpha(\omega)$ at each frequency according to

$$\alpha = \alpha_r + j\alpha_i = \omega C_{BC}\left(-\operatorname{Im}\left[\frac{H_{21} + H_{12}}{H_{22}}\right] + j \operatorname{Re}\left[\frac{H_{21} + H_{12}}{H_{22}}\right]\right) \tag{20}$$

The result for $|\alpha(\omega)|$ is shown in Fig. 6 and the result for $\angle\alpha(\omega)$ is shown in Fig. 7. The symbol points are the values directly calculated from the S-parameters using the approach presented in this paper. The solid lines are calculated curves obtained by fitting the following expression [6] to those points:

$$\alpha(\omega) = \frac{\alpha_0}{1 + \frac{j\omega}{\omega_\beta}} e^{-j\omega[(m\tau_B/1.2) + (\tau_C/2)]} \tag{21}$$

where τ_B is the base transit time and τ_C is the collector transit time assuming constant velocity throughout the base-collector space-charge region. This assumption is justified particularly for power HBT designs where a very thick and low-doped pre-collector is used. A calculation of the effective carrier velocity (v) from the extracted τ_C values and using depletion layer thickness (W_{BC}) values estimated on the basis of the depletion layer approximation, shows that v is not significantly higher than v_{SAT} and does not strongly depend on V_{CE}. Also in (21), $\omega_\beta = 1.2/\tau_B$ is the 3 dB frequency of the α expression, and $m = 0.22$ is the empirical factor employed to match the phase of the 3 dB roll-off approximation for $\alpha(\omega)$ to its more accurate hyperbolic secant representation. As can be seen, the directly calculated values follow well the trends presented by the theoretical model of (21). This is to the

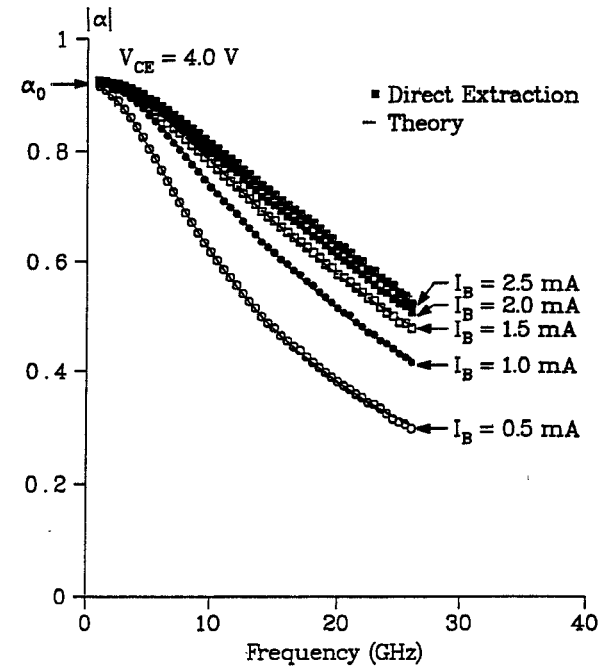

Fig. 6. Intrinsic base transport factor magnitude versus frequency showing excellent agreement with the single pole approximation as well as the gain improvement with bias.

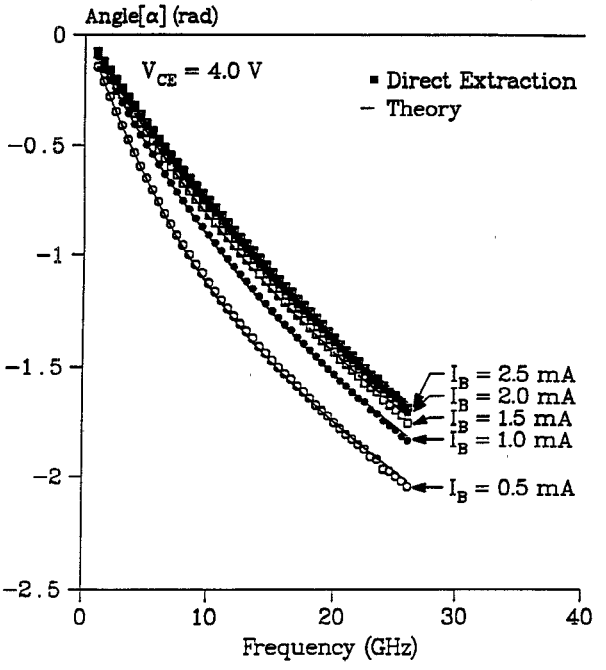

Fig. 7. Intrinsic base transport factor phase angle versus frequency showing excellent agreement with the single pole approximation as well as the gain improvement with bias.

best of our knowledge the first demonstration of direct calculation from measured S-parameters of the frequency dependence of the intrinsic base transport factor $\alpha(\omega)$. Traditional techniques have relied on fitting and/or separate measurement for parasitic de-embedding before intrinsic small-signal parameters of this kind are extracted.

F. Base and Collector Transit Times (τ_B, τ_C)

The only unknowns in the expression for the magnitude $|\alpha(\omega)|$ shown in Fig. 6, are the dc value of the transport factor, α_0, and the alpha 3 dB frequency, ω_β:

$$|\alpha(\omega)| = \frac{\alpha_0}{\sqrt{1 + \dfrac{\omega^2}{\omega_\beta^2}}}. \tag{22}$$

By taking α_0 to be the value approached by $|\alpha(\omega)|$ at low frequency, we are left with only one unknown and can calculate ω_β (and therefore the base transit time $\tau_B = 1.2/\omega_\beta$) directly at each frequency using

$$\tau_B = \frac{1.2\sqrt{\alpha_0^2 - |\alpha(\omega)|^2}}{\omega|\alpha(\omega)|}. \tag{23}$$

The phase angle of the base transport factor, $\angle\alpha(\omega)$, is shown in Fig. 7 and depends only on τ_B and the collector transit time τ_C:

$$\angle\alpha(\omega) = -\tan^{-1}\left(\frac{\omega}{\omega_\beta}\right) - \omega\left[\frac{m\tau_B}{1.2} + \frac{\tau_C}{2}\right]. \tag{24}$$

With τ_B known at each frequency from (23), we may then use $\angle\alpha(\omega)$ to calculate τ_C at each frequency using

$$\tau_C = \frac{2}{\omega}\left[-\angle\alpha(\omega) - \tan^{-1}\left(\frac{\omega\tau_B}{1.2}\right)\right] - \frac{m\tau_B}{1.2}. \tag{25}$$

As is shown in Fig. 8 since $\tau_B >> \tau_C$, the transit time in these devices is dominated by base diffusion of minority carriers and both base and collector transit times exhibit bias dependencies. The collector transit time increases with increased reverse bias on the base-collector junction as is expected as that depletion region thickness swells, and compares well with estimates of $\tau_C = W_{BC}/2v_{sat}$ based on depletion approximation treatment of the base-collector space charge layer as shown in Table I. The slight bias dependence of τ_B with V_{CE} is not completely understood at this time, but is unlikely to show up as a result of the variations in τ_C. This can be seen from (21) where the base-collector transit time τ_C contributes only to the phase of $\alpha(\omega)$ and not to the magnitude $|\alpha(\omega)|$ from which we calculate τ_B.

G. Base-Emitter Junction Impedance and Emitter Parasitics

Once $\alpha(\omega)$ is found, we can apply the expression for device input resistance r_e, found in [6] as

$$r_e = R_{BE}(1 - \alpha_0 e^{-j\omega[(m\tau_B/1.2) + (\tau C/2)]}) \tag{26}$$

where R_{BE} is the base-emitter junction resistance. The direct calculation of $Z_{BE} + z_E$ according to (7) yields the real and imaginary values for a system of two equations and four unknowns (R_{BE}, C_π, R_E, and L_E) in the emitter leg of the T-model. Unfortunately, we are unable to calculate any single element exactly because of the number of unknowns in this block of the circuit, but can signifi-

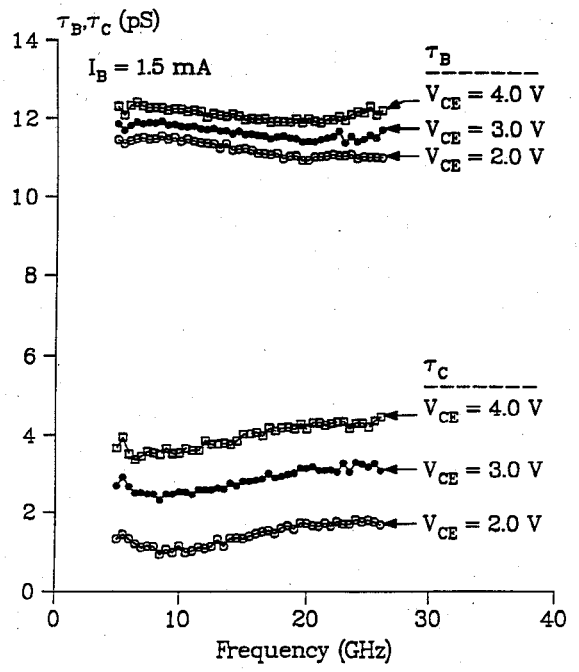

Fig. 8. Base and collector transit times versus frequency showing the increase in transit time with V_{CE}.

cantly reduce the error for a fitting routine by fixing the $\alpha(\omega)$ expression extracted above, and applying optimization to this reduced subcircuit with added confidence.

IV. Isolating the Impact of Element Values on High-Frequency Performance—Importance of Transit Time Versus Charging Time Effects

Using the developed technique one can evaluate the importance of each parameter in the overall determination of the HBT high-frequency response. In particular, the formalism may be used as a tool to evaluate the f_T intercept where $|H_{21}| = 1$ and the reasons that it occurs where it does in frequency. The transit times and RC product time constants all contribute in a complicated way to produce the frequency response of the HBT. By investigating the expression for H_{21} given for the T-Model in (2), we may isolate those key elements that contribute to the $|H_{21}|$ roll-off, and which are the most important in determining the f_T value. By evaluating the magnitude of H_{21}, we see from equation (2):

$$|H_{21}| = \left|\frac{X}{Y - X}\right| = \left|\frac{X/Y}{1 - (X/Y)}\right| \tag{27}$$

where $X = \alpha Z_{BC} - Z_{BE} - z_E$ and $Y = Z_{BC} + z_C$. At the frequency where $|H_{21}| = 1$, one obtains the constraint that

$$\left|\frac{X}{Y}\right| = \left|1 - \frac{X}{Y}\right|. \tag{28}$$

And equating real and imaginary parts of this expression allows reduction of the constraint which holds true at $f = f_T$:

$$\mathrm{Re}[\alpha] - \frac{1}{2} = \mathrm{Re}\left[\frac{Z_{BE} + z_E + \alpha z_C}{Z_{BC} + z_C}\right]. \tag{29}$$

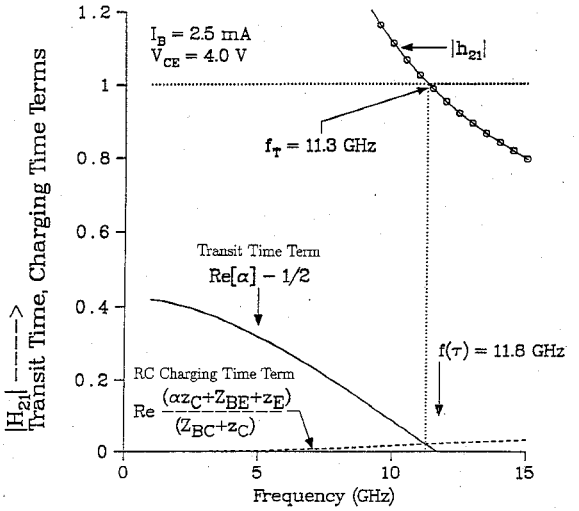

Fig. 9. Impact of transit times versus RC charging times in determining f_T. Current gain (H_{21}), transit time term ($\mathrm{Re}[\alpha] - 1/2$), and RC charging time term ($\mathrm{Re}[(Z_{BE} + z_E + \alpha z_C)/(Z_{BC} + z_C)]$) versus frequency. $\mathrm{Re}[\alpha] = 1/2$ indicates the f_T due ONLY to transit time limitations.

This evaluation has separated out the transit time contribution to f_T expressed as $\mathrm{Re}[\alpha] - \frac{1}{2}$ from the rest of the RC product time constants making up the rest of (29). The RC term includes $\alpha(\omega)$ also, but it is coupled through the extrinsic series parasitics and constitutes more the impact of series R–L degradation of f_T, so that when $z_C = 0$, the coupling with $\alpha(\omega)$ is eliminated. We see in Fig. 9 that the frequency where $\mathrm{Re}[\alpha] - \frac{1}{2}$ equals the real part of the RC charging term corresponds to the f_T intercept. We may also see that in the absence of RC charging terms, the frequency at which $\mathrm{Re}[\alpha] - \frac{1}{2} = 0$ constitutes the maximum f_T due only to the frequency dependence of $\alpha(\omega)$ and therefore represents the ultimate device performance due only to transit time limitations. By noting that the total delay time for the HBT ($\tau_{EC} = \dfrac{1}{2\pi f_T}$ is the sum of the total transit delay (τ_F) and charging time (τ_{RC}), we are able to express this transit time limited frequency $f(\tau)$ in terms of the total carrier delay time τ_F alone with $\tau_{RC} = 0$ as

$$f(\tau) = \frac{1}{2\pi\tau_F} = \frac{1}{2\pi(\tau_B + \tau_C/2)}. \tag{30}$$

The inclusion of Z_{BE}, Z_{BC}, z_C, and z_E serves to add delay, and the real part of the RC charging term increases with frequency serving to reduce the frequency at which the two terms intersect, and lowering the overall measured f_T. For the device presented here in Fig. 9 we see that the measured f_T of 11.3 GHz corresponds to the point at which the condition of (29) holds, and therefore, where the two curves representing $\mathrm{Re}[\alpha] - 0.5$ and $\mathrm{Re}[(Z_{BE} + z_E + \alpha z_C)/(Z_{BC} + z_C)]$ intersect. The transit time limited frequency is represented by the frequency at which $\mathrm{Re}[\alpha] - 0.5 = 0$ and occurs at 11.8 GHz, which is only slightly higher than the measured f_T. This figure demonstrates that while the RC factor serves to decrease the measured f_T, it is the transit times that have the more significant impact in lowering the overall frequency response.

V. Conclusions

In summary, we have demonstrated a formalism for direct calculation of the HBT equivalent circuit from measured S-parameters without test structure characterization and a minimum of numerical fitting. Resistances, capacitances, the base transport factor, base and collector transit times are all analytically derived and their bias dependence investigated for clues to the impact they have on the overall device performance. A new approach to calculating the individual components of the HBT equivalent circuit, and how they determine the frequency dependence of $|H_{21}|$, and therefore f_T, is also investigated along with an analysis separating the transit times and RC charging times to determine the impact of RC delays, and the ultimate performance of the HBT based on the limitations imposed by the transit times alone. This approach can serve as a useful tool toward optimization of process technologies and HBT high-speed performance, revealing the factors that limit device performance and allowing direct insight into the HBT device physics.

References

[1] R. L. Vaitkus, "Uncertainty in the values of GaAs MESFET equivalent circuit elements extracted from two-port scattering parameters," in *Proc. IEEE/Cornell Conf. on High-Speed Semiconductor Devices and Circuits*, 1983, pp. 301–308.

[2] D. Costa, W. U. Liu, and J. S. Harris, "Direct extraction of the AlGaAs/GaAs heterojunction bipolar transistor small-signal equivalent circuit," *IEEE Trans. Electron Devices*, vol. 38, pp. 2018–2024, Sept. 1991.

[3] H. Cho and D. E. Burke, "A simple model for distributed base impedance with ac verification using S-parameter measurements," in *IEEE 1990 Bipolar Circuits and Technology Meeting*, 5.3, pp. 106–109.

[4] D. Pehlke and D. Pavlidis, "Direct calculation of the HBT equivalent circuit from measured S-parameters," in *1992 IEEE MTT-S Int. Microwave Symp. Dig.*, Albuquerque, NM, June 1–5.

[5] D. Pehlke and D. Pavlidis, "Critical issues in process technology for high-speed self-aligned GaAs/AlGaAs heterojunction bipolar transistors," in *Dig. GaAs Manufacturing and Technology Conf.*, Reno, NV, April, 1991, pp. 93–96.

[6] A. P. Laser and D. Pulfrey, "Reconciliation of methods for estimating f_{MAX} for microwave heterojunction transistors," *IEEE Trans. Electron Devices*, vol. 38, pp. 1685–1692, Aug. 1991.

[7] R. L. Pritchard, *The Electrical Characteristics of Transistors*. New York: McGraw-Hill, 1967, p. 233.

David R. Pehlke received the S.B. degree in electrical engineering from M.I.T. in 1986, the M.S.E. degree in electrical engineering from the University of Michigan in 1988, and is currently fulfilling the requirements of the Doctoral program in the University of Michigan's Center for High-Frequency Microelectronics. His current work involves GaAs/AlGaAs HBTs with an emphasis on Process Technology Development in the areas of Self-Aligned Structures, Carrier Transport Mechanisms in HBTs, and DC and RF Parameter Extraction Techniques for Determining the Physics of Limitations to HBT Performance.

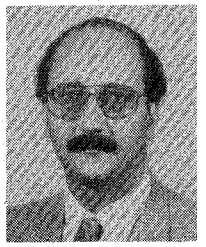

Dimitris Pavlidis (S'73–M'76–SM'83) has been Professor of Electrical Engineering and Computer Science at the University of Michigan, Ann Arbor, since 1986. He received the B.Sc. degree in physics from the University of Patras, Patras, Greece, in 1972 and the Ph.D. degree from the University of Newcastle, Newcastle-upon-Tyne, England, in 1976. He continued as Postdoctoral Fellow at Newcastle until 1978, engaged in work on microwave semiconductor devices and circuits. In 1978 he joined the High Frequency Institute of the Technical University of Darmstadt, West Germany, working on III-V devices and establishing a new semiconductor technology facility. In 1980 he worked at the Central Electronic Engineering Research Institute, Pilani, India, as UNESCO consultant.

During 1980–1985 he was Engineer and Manager of the GaAs Monolithic Microwave Integrated Circuits (MMIC) Group of Thomson-CSF, Corbeville, France. In this capacity he was responsible for projects on monolithic power and broad-band amplifiers, tunable oscillators, optical pre-amplifiers, phase shifters, attenuators, their technology and process evaluation, and the establishment of a component library for MMIC applications. His publications are in microwave semiconductor devices and circuits and he holds 6 patents on MMIC applications. His current research interests cover the design and fabrication of HEMT's, HBT's, strained III-V microwave devices and monolithic heterostructure integrated circuits.

In 1990 Dr. Pavlidis was awarded the European Microwave Prize for his work on InP based monolithic integrated HEMT amplifiers. In 1991 he was awarded the decoration of "Palmes Académiques" in the order of "Chevalier" by the French Ministry of National Education for distinguished work in the field of education. In 1992 he received the JSPS Fellowship by the Japanese government and the Humboldt Research Award for Distinguished Senior US Scientists.